Investigation of Fundamental EMI Source Mechanisms Driving Common-Mode Radiation from Printed Circuit Boards with Attached Cables

David M. Hockanson, *Student Member, IEEE,* James L. Drewniak, *Member, IEEE,* Todd H. Hubing, *Senior Member, IEEE,* Thomas P. Van Doren, *Member, IEEE,* Fei Sha, *Member, IEEE,* and Michael J. Wilhelm

***Abstract*— Fundamental EMI source mechanisms leading to common-mode radiation from printed circuit boards with attached cables are presented in this paper. Two primary EMI source mechanisms have been identified: one associated with a differential-mode voltage and another associated with a differential-mode current, both of which result in a common-mode current on an attached cable. These mechanisms can be used to relate printed circuit layout geometries to EMI sources. The two mechanisms are demonstrated through numerical and experimental results, and an example from a production printed-circuit design is presented.**

I. Introduction

INCREASING EMI clock speeds and edge rates, as well as the increasing density of digital designs, pose greater challenges in producing systems that readily comply with FCC and CISPR EMI limits. Common-mode radiation from printed circuit boards (PCB's) with attached cables is a primary concern in meeting EMI specifications. The cable is typically one part of an antenna with the noise source located on the PCB or an equivalent noise source located at the connector. The other half of the "dipole-type" radiating structure can be more difficult to determine, but might include an extended portion of the ground or other metal structures of significant electrical extent on the PCB directly attached or effectively coupled to the PCB at RF frequencies. While common-mode radiation from cables attached to PCB's is a well-known problem, the fundamental mechanisms by which signal or differential-mode sources produce or induce common-mode currents on the cables are not well understood. This makes diagnosing common-mode radiation problems on hardware with attached cables difficult. A lack of knowledge of fundamental EMI sources also makes anticipating potential EMI problems at the design stage troublesome. Designs with unidentified EMI sources often require numerous time-consuming and costly retrofits. A knowledge of EMI source mechanisms and their relationship to layout geometries is necessary to determine the essential features that must be modeled to estimate emissions and provide direction for reducing EMI in a design.

Manuscript received April 10, 1996; revised June 25, 1996. This work was supported in part by General Motors and the National Science Foundation through a graduate research fellowship.

D. M. Hockanson, J. L. Drewniak, T. H. Hubing, and T. Van Doren are with the Department of Electrical Engineering, Electromagnetic Compatibility Laboratory, University of Missouri, Rolla, MO 65401 USA.

F. Sha is with the Northern Jaotong University, EMC Research Section, Beijing 100044 China.

M. J. Wilhelm is with Motorola Inc., Ft. Worth, TX 76137 USA.

Publisher Item Identifier S 0018-9375(96)08896-5.

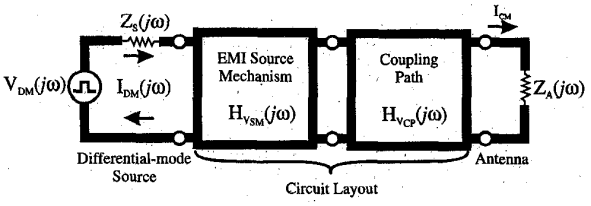

Fig. 1. Components of an EMI problem.

Paul has emphasized and demonstrated the need to consider and model common-mode currents in order to adequately predict radiation from printed circuit designs [1], [2]. Hubing *et al.*, as well as Hardin *et al.*, demonstrated the importance of circuit asymmetries in producing common-mode radiation. References [5]–[10] have shown that voltage drops on signal return conductors can result in common-mode radiation as a result of driving two portions of extended ground against each other. Drewniak *et al.* have also shown with production hardware that potential differences between portions of extended ground structures can result from parasitically coupled noise currents returning to their source [11].

Two fundamental EMI source mechanisms that result in common-mode current on a cable attached to a PCB are presented in this paper. Examples of currents induced on wire extensions from a circuit using a numerical electromagnetics code are given for these two mechanisms. Simple wire circuits that are representative of PCB geometries were constructed to demonstrate the mechanisms and to illustrate the dominance of one over the other in different cases. Finally, experimental results for a production PCB design with a single processor are presented to illustrate the EMI source mechanisms.

II. Fundamental EMI Source Mechanisms

An EMI problem can be characterized in terms of:

1) a specific differential-mode source (such as an IC);
2) an EMI antenna;
3) an EMI source mechanism;
4) a coupling path as shown in Fig. 1.

An EMI noise-source is defined here as an unintentional voltage that drives an EMI antenna and results in radiation. An IC may be the source from which the radiated energy

originates; however, the EMI noise source exists where a voltage drop causes an EMI antenna to be excited. The specific IC that is directly responsible for producing the differential-mode signal that couples to an EMI antenna can be determined in practice through a process of selectively enabling and disabling portions of the design. This approach can be arduous and time-consuming when working with prototype hardware. At the design stage, it is usually difficult to determine which devices will lead to EMI problems, and broad design maxims are typically invoked to provide guidance with design and layout decisions.

The EMI antenna can similarly be determined with working hardware by trial-and-error. In high-speed digital hardware, with clock speeds ranging from a few megahertz to a few hundred megahertz, cables and seams remain the primary EMI antennas. With the increasing use of conducting enclosures to contain electromagnetic energy, and increasing clock and edge rates, radiation through perforations in the enclosure are becoming common EMI problems. Although radiation from slots and seams can be a significant problem, the cables attached to a system are generally the best EMI antennas, particularly at frequencies below 500 MHz. At resonance, the resulting input impedance for these EMI antennas is on the order of tens of ohms to a few hundred ohms [12]. As a result of the relatively low antenna input impedance, the cable antennas can be more effectively driven by low-impedance noise sources. In the case of common-mode radiation from cables, the EMI antenna is a "dipole-type" antenna, i.e., an "antenna" with two distinct conductor halves at different RF potentials that are driven against each other to produce radiation. One part of the antenna is typically the cable, and the other part might be a conducting enclosure, PCB power or ground plane, a heatsink, portions of extended ground, or other conductors of significant electrical extent attached or capacitively coupled to the PCB. Cables attached to a system are always considered potential EMI antennas, but it is often difficult to anticipate the other part of the antenna at the design stage.

The effective EMI noise source, or equivalent noise source in a reduced lumped element model, and the path by which this effective source is coupled to the EMI antenna are typically the most difficult aspects of an EMI problem with working hardware. Further, they are also often difficult to anticipate at the design stage. Two fundamental EMI source mechanisms have been investigated and are denoted *current-* and *voltage-*driven mechanisms to distinguish the input that provides the driving mechanism for the common-mode current on the attached cable.

A. Current Driven Mechanisms

A wire circuit example that illustrates the physics of the current-driven mechanism is shown in Fig. 2(a). The time-varying current I_{DM} flowing in the circuit loop generates a time-varying magnetic flux. The flux may couple to other possible current paths, including common-mode current paths. The *emf* driving the current in the common-mode path may be represented as a voltage dropped across an equivalent inductance. This voltage drop provides a source that can drive common-mode current on the extended lower conductor as shown, resulting in common-mode radiation. Work with production printed circuit designs has shown that current-driven EMI sources are frequently encountered in practice. In high-speed designs, it is often difficult to realize a sufficiently low-impedance connection between two portions of extended ground, as represented by L_{Return} in Fig. 2(a).

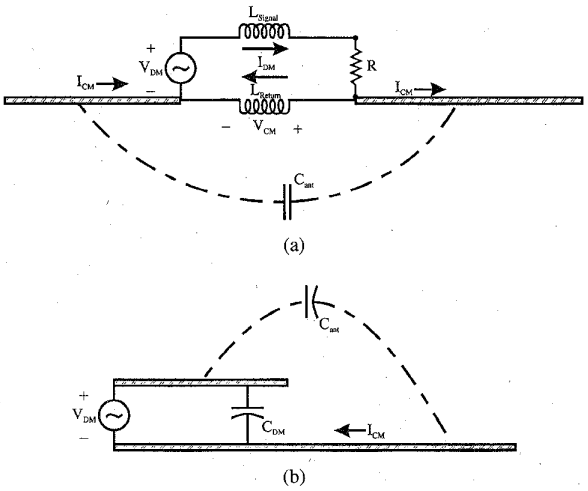

Fig. 2. Wire circuit examples illustrating the physics of the (a) current- and (b) voltage-driven mechanisms.

The effective EMI noise source in Fig. 2(a) is a result of significant differential-mode current in the circuit loop for low-impedance loads (e.g., 50 Ω). The common-mode current below resonance on an electrically small EMI antenna in the current-driven case is approximately $I_{CM} \sim j\omega C_{ant} V_{CM}$, where C_{ant} is the capacitance between the two extensions of the lower conductor. Since V_{CM} results from the differential-mode signal I_{DM} through the finite impedance of the signal return path, $V_{CM} \sim j\omega L_{return} I_{DM}$. Assuming that R is much larger than $j\omega L_{loop}$ below resonance, $I_{DM} \approx V_{DM}/R$. Then the common-mode current on the extended lower conductor is approximately $I_{CM} \sim -\omega^2 C_{ant} L_{return} V_{DM}/R$. The current-driven EMI source is then expected to produce a 40 dB/decade variation with frequency below the antenna resonance. While the EMI source mechanism that drives the EMI antenna for a printed circuit design is often current-driven, the coupling path between the differential-mode source and EMI antenna is seldom as simple as that depicted in Fig. 2(a).

B. Voltage Driven Mechanisms

A wire circuit example illustrating the voltage-driven mechanism is shown in Fig. 2(b). In this case, the differential-mode voltage provides the driving source that results in common-mode current. A differential-mode current results from the impedance between the upper conductor and the portion of the reference conductor directly beneath the upper conductor. This differential-mode current path is represented schematically by C_{DM} in Fig. 2(b). The extension of the return conductor beyond that of the signal conductor results in additional capacitance between the two conductors and

an alternate current path. This alternate current path then results in common-mode current and common-mode radiation. In Fig. 2(b) the antenna capacitance is depicted between the upper conductor and the extension of the lower conductor. However, realistically it may exist between the upper conductor and any other reference conductor or extended ground. If the conductors are electrically short, the common-mode current in the voltage-driven case is approximately $I_{CM} \sim j\omega C_{ant} V_{DM}$, where C_{ant} is the capacitance between the upper conductor in Fig. 2(b) and the portion of the lower conductor that extends beyond the length of the upper conductor. A 20 dB/decade variation with frequency results, which agrees with experimental and numerical examples given below. The voltage-driven EMI source mechanism is more intuitive and better understood than the current-driven mechanism. This is why few metal structures of significant electrical extent are left "ungrounded" in high-speed digital designs.

The dashed lines and parasitic capacitance shown in Fig. 2 represent the displacement current path that results in common-mode current on the EMI antenna below the antenna resonance. For dipole-type EMI antennas within a conducting enclosure, the antennas are expected to be electrically small at frequencies below a few-hundred MHz for both the current- and voltage-driven cases. For greater clock speeds and typical cable lengths of a meter (power and peripheral cables), the EMI dipole antenna will have resonant dimensions for relatively low order harmonics, with an input impedance on the order of tens of ohms to a few hundred ohms. However, as long as the source geometry remains electrically small, the EMI source mechanism may continue to be categorized as voltage- or current-driven.

The EMI noise sources shown in Fig. 2 are directly coupled to the EMI antenna for simplicity and clarity. Effectively, $H_{V_{CP}} = 1$ in Fig. 1. However, in practice, the coupling path is seldom this simple or direct, but includes parasitic capacitances and inductances that are a function of the board layout, significant metal structures, grounding, etc. As a consequence, the frequency response of the coupling path can be complicated, and in general a source cannot be identified as voltage- or current-driven based on its radiated spectrum.

III. Numerical Results

Numerical simulations on simple wire circuit configurations were pursued to test the physics described above. One circuit configuration is shown in Fig. 3. The simulations were performed using the numerical electromagnetics code (NEC) [13]. NEC is a proven full-wave electromagnetic-modeling code based on the method of moments that is superior for wire geometries. While the circuits that were investigated were simple, they are representative of the dipole-type antennas that typically arise with common-mode radiation problems in printed circuit designs. In Fig. 3 the geometry is short in terms of the free-space wavelength, which is greater than 3 m for all simulation frequencies. The model is electrically short to demonstrate the physics of the noise-source mechanisms, but in practice EMI antennas may be any size. The wire radius in the circuit is 0.8 mm. The 1 cm vertical wires were modeled

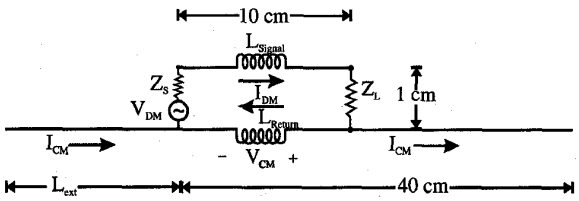

Fig. 3. Representatve wire circuit geometry investigated using NEC.

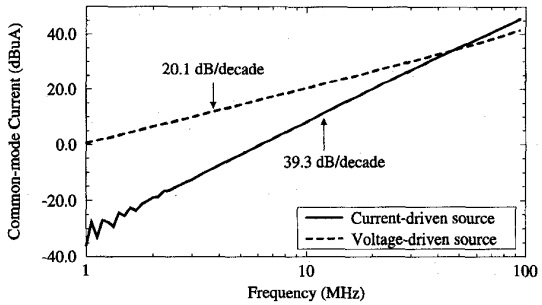

Fig. 4. Frequency variation of the common-mode current induced on a cable for the current-driven, and voltage-driven noise-source mechanisms.

with five segments in the NEC geometry description file, while the horizontal wires were modeled with segments 1 cm long. The common-mode current in the circuit was computed by adding the current on the upper conductor to that on the lower conductor [14]. First, the frequency dependence for the two mechanisms was investigated. A 50 Ω source impedance was implemented with a 1 V source, and $L_{ext} = 30$ cm. A 50 Ω source impedance was modeled so that the loop impedance associated with the inductance in the loop was small relative to 50 Ω (for $Z_L = 0$) over the frequency range 1–100 MHz, and the differential-mode current remained constant. The common-mode current 15 cm to the right of Z_L as a function of frequency was calculated from the full-wave simulation results and shown for $Z_L = 0$ (current-driven), and $Z_L = \infty$ (voltage-driven) in Fig. 4. The common-mode current on the cable increases by 39.3 dB/decade for the current-driven mechanism, and 20.1 dB/decade for the voltage-driven mechanism, which is consistent with the previously discussed physics.

The magnitude of the common-mode current over the circuit length was compared for the two mechanisms as well. The source frequency was 30 MHz, the source voltage 1 V, and the source impedance $Z_s = 50$. The magnitude of the common-mode current for the open circuit ($Z_L = \infty$) case of Fig. 3 with $L_{ext} = 30$ cm is shown in Fig. 5. The driving source for the common-mode antenna is V_{DM}, and the extent of the two halves of the EMI antenna is sufficient to result in a significant common-mode current, with a peak current of approximately 75 μA. The common-mode current is a result of the differential-mode voltage source, i.e., a voltage-driven mechanism. The common-mode current is asymmetric about the center of the configuration which indicates that no current-driven source is present. NEC simulations for the voltage-driven case with $L_{ext} = 0$ showed a peak common-mode current of 127 μA.

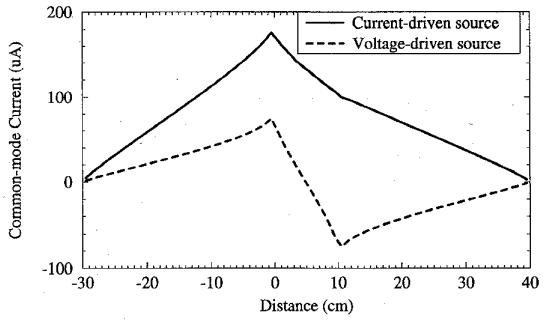

Fig. 5. Common-mode current computed using NEC for open and short circuit cases of Fig. 3. The origin is taken to be the location of the source.

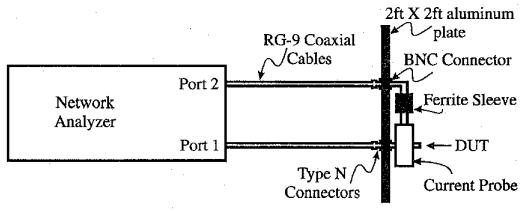

Fig. 6. Experimental configuration for investigation of circuit geometries with the HP8753C network analyzer.

The common-mode current computed for the current-driven mechanism ($Z_L = 0$) for the wire circuit geometry of Fig. 3, with $L_{ext} = 30$ cm is shown in Fig. 5. Again, the differential-mode current in the finite-impedance lower conductor of the differential-mode loop results in a voltage drop along this length. The equivalent noise-voltage source that is distributed over the length of the conductor then drives the EMI antenna, which is comprised of the two extensions of the lower conductor. The peak common-mode current is 175 μA.

IV. Experimental Results

Simple passive wire-circuit test configurations were constructed to investigate the fundamental mechanisms of common-mode radiation described in the previous section. An HP8753C network analyzer was employed for measuring $|S_{21}|$. The experimental configuration is illustrated schematically in Fig. 6. Port 1 of the network analyzer is the driving source for the wire circuit, and the output of a common-mode current probe was input to Port 2. The effective source impedance for the circuit was the 50 Ω impedance of the network analyzer. A 2 ft $\times$ 2 ft square aluminum plate was used in all the measurement procedures in order to obtain a sufficiently large common-mode current to measure and to provide a test environment for making repeatable measurements. The measured common-mode current was not a function of the network analyzer cable dressing when the aluminum plate was employed. The common-mode current was measured using a Fischer F-62 (10 MHz–1 GHz) current probe. A ferrite sleeve (200 Ω at 100 MHz) was employed to reduce coupling to the current probe. The transfer impedance of the current probe was included in the calibration procedures using the error correction capabilities of the HP8753C network analyzer.

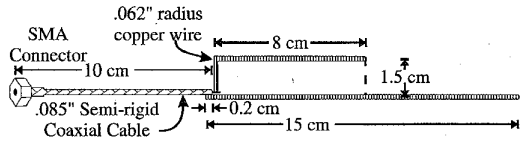

Fig. 7. Wire-circuit configuration for demonstrating the voltage- and current-driven mechanisms in printed circuit geometries.

The current- and voltage-driven mechanisms were investigated for the wire circuit shown in Fig. 7. While the circuit geometry is not physically very similar to typical printed-circuit geometries, the measurements on the circuit demonstrate the fundamental physics under investigation. The circuit source was provided by the network analyzer, and the common-mode current measured as previously described. The results for both open- and short-circuit loading conditions are shown in Fig. 8. The open-circuit results are shown in Fig. 8(a). The data shows an increase of common-mode current with frequency of 20.5 dB/decade, which is consistent with the physics for voltage-driven source. The common-mode path for the geometry of Fig. 7 (below the antenna resonance frequency) is a displacement-current path between the upper-conductor and the coaxial cable. By a current-divider equation, if the differential-mode capacitance [C_{DM}, see Fig. 2(b)] is increased, less common-mode current should flow. A 1 cm wide, 8 cm copper strip was attached to the lower-conductor directly beneath the upper-conductor. Curve 4 of Fig. 8(a) shows a drop in common-mode current of approximately 1 dB results from the addition of the copper strip. Similarly, when a copper strip is placed on the upper-conductor, the common-mode or antenna capacitance is increased and more common-mode current flows as shown in Curve 1. The increase in common-mode current for Curve 1 is approximately 3 dB. When copper strips are added to both conductors, the change in the antenna capacitance dominates as shown by Curve 2, which also has an increase in common-mode current from Curve 3 of approximately 3 dB.

The short-circuit case demonstrates the current-driven source mechanism as shown in Fig. 8(b). A 1.5 cm long 0.062 in radius copper wire was used to provide a short located along the dotted line in Fig. 7. The results near 10 MHz were at the limit of the dynamic range of the test setup; hence, the noise in the data at low frequencies. Curve 3 shows the data for the short-circuit case with bare wires. The common-mode current increases with frequency at 11.8 dB/octave (approximately 40 dB/decade) between 20–40 MHz. A copper strip attached to the upper-conductor lowers the value of L_{signal} [see Fig. 2(a)]. The voltage distributed around the loop is then dropped primarily across L_{return}, resulting in a larger common-mode voltage-source. Therefore, more common-mode current is driven onto the EMI antenna as shown by Curve 1. The common-mode current is increased by approximately 2 dB over the base case of Curve 3. Similarly, a copper strip on the lower-conductor should lower the common-mode voltage-source resulting in less common-mode current. Curve 4 consequently shows a decrease in common-mode current of approximately 2 dB. When a copper strip is added to both conductors the effects approximately cancel each

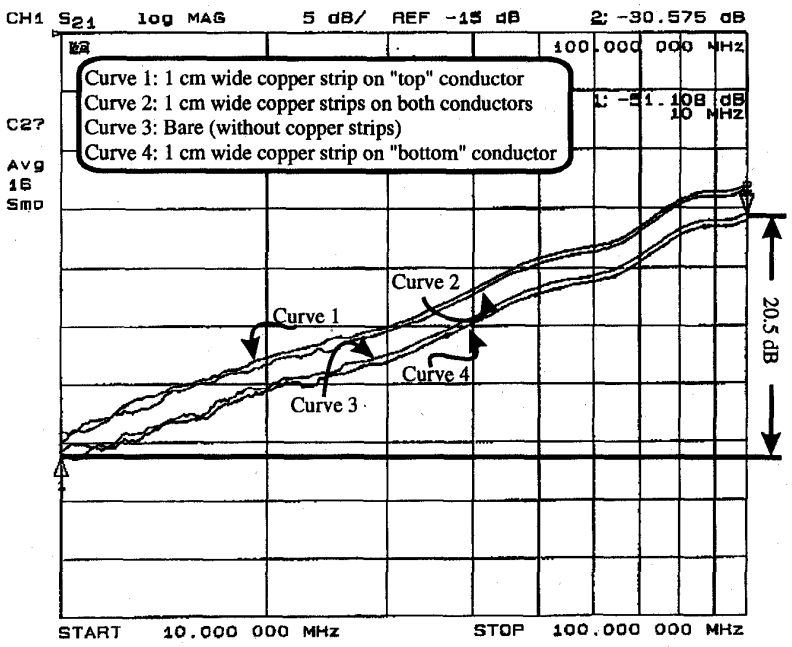

(a)

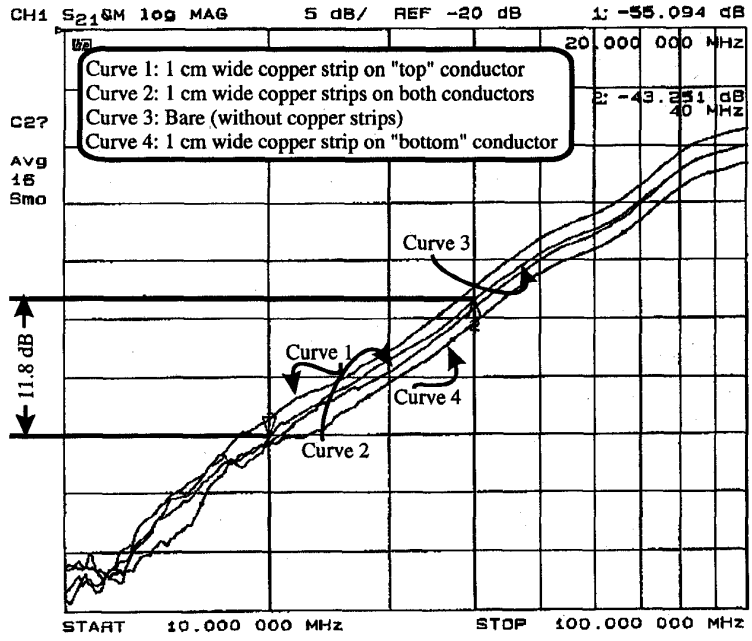

(b)

Fig. 8. (a) Open-circuit and (b) short-circuit results measured with the HP8753C network analyzer for the wire-circuit geometry of Fig. 7.

other. Consequently, Curves 2 and 3 are very similar in the measured frequency range.

The driving source for the current-driven mechanism is the voltage drop incurred as a result of the differential-mode current through the finite signal return impedance (inductance), and, hence, the equivalent driving voltage for the cable can be reduced by widening the ground plane. This was investigated experimentally with the wire circuit geometry over a ground conductor shown in Fig. 9(a). The common-mode current at the SMA connector was measured for a 1, 3, 5, 10, and 14 cm wide signal return conductor and is shown in Fig. 9(b). The current is limited by the 50 Ω source impedance in series with the loop inductance. Using the approximate formula for a wire over an infinite ground plane, the loop impedance at 100 MHz is approximately $j37\,\Omega$. As the width of the signal return conductor is increased, the measured common-mode current decreases, which is consistent with a decreasing common-mode driving source.

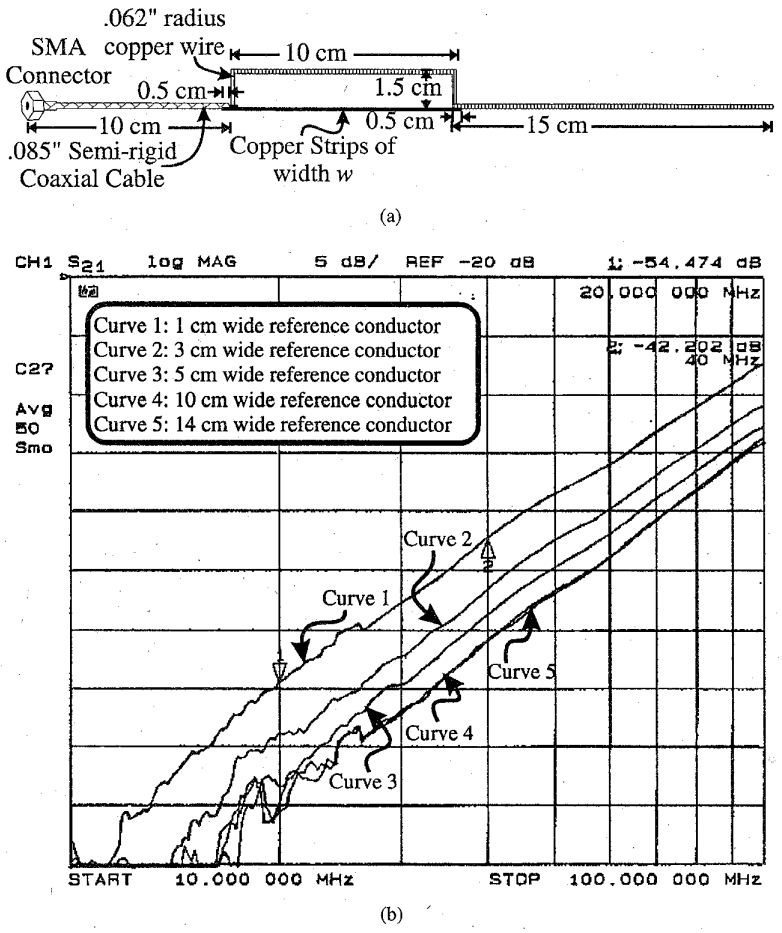

Fig. 9. (a) Circuit geometry for investigating the dependence of the current driven mechanism on the width of the signal return conductor. (b) Data for signal return conductor widths of 1, 3, 5, 10, and 14 cm.

V. A Practical Application

The principles detailed in the above sections were applied to reduce the common-mode radiation from a production printed circuit design. The circuit, denoted the daytime running lamp (DRL) module, produced significant common-mode radiation in a frequency band around 50 MHz. A schematic of the experimental configuration is shown in Fig. 10(a). The DRL module was powered by a 12 V bench power supply with 1 m long power and ground leads. A 1 m wire was also connected to the photocell input (which is connected to V_{CC}) and left unterminated to simulate the high impedance loading associated with night-time conditions. The DRL module is a two-sided PCB design with a single IC 2 MHz microprocessor. The PCB dimensions were approximately 6.5× 8.5 cm^2. The common-mode current on the three attached leads was measured 6 in from the DRL module with a Fischer F-33-1 (200 kHz–250 MHz) current probe connected to the spectrum analyzer, and shown in Fig. 11. Significant common-mode current on the cable bundle was measured in a band around 50 MHz. Neither the 12 V power nor the photocell input lead was capacitively decoupled to the battery ground at the connector.

A simple 0.085 in semi-rigid coaxial cable probe with an extended center conductor was employed for measuring the RF noise on the 5 V side of the dc power bus. The center conductor of the probe was placed in contact with the 5 V conductor, and the noise current return path was capacitively coupled from the coaxial probe outer shield to the circuit conductor

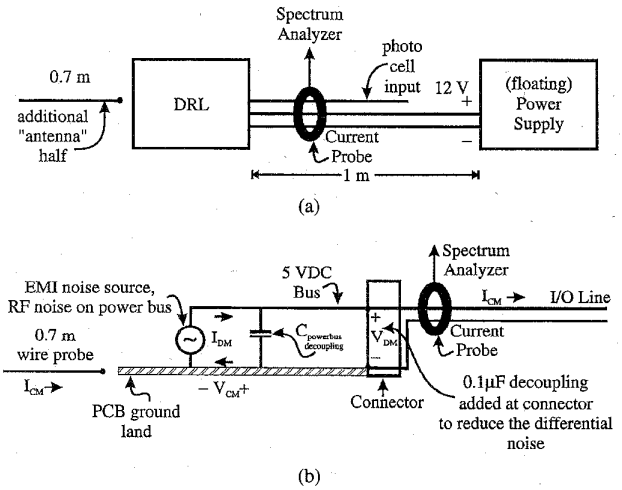

Fig. 10. (a) Experimental configuration for common-mode current measurements on the leads to the DRL module. (b) Reduced circuit model illustrating the fundamental mechanisms leading to common-mode radiation for the DRL module.

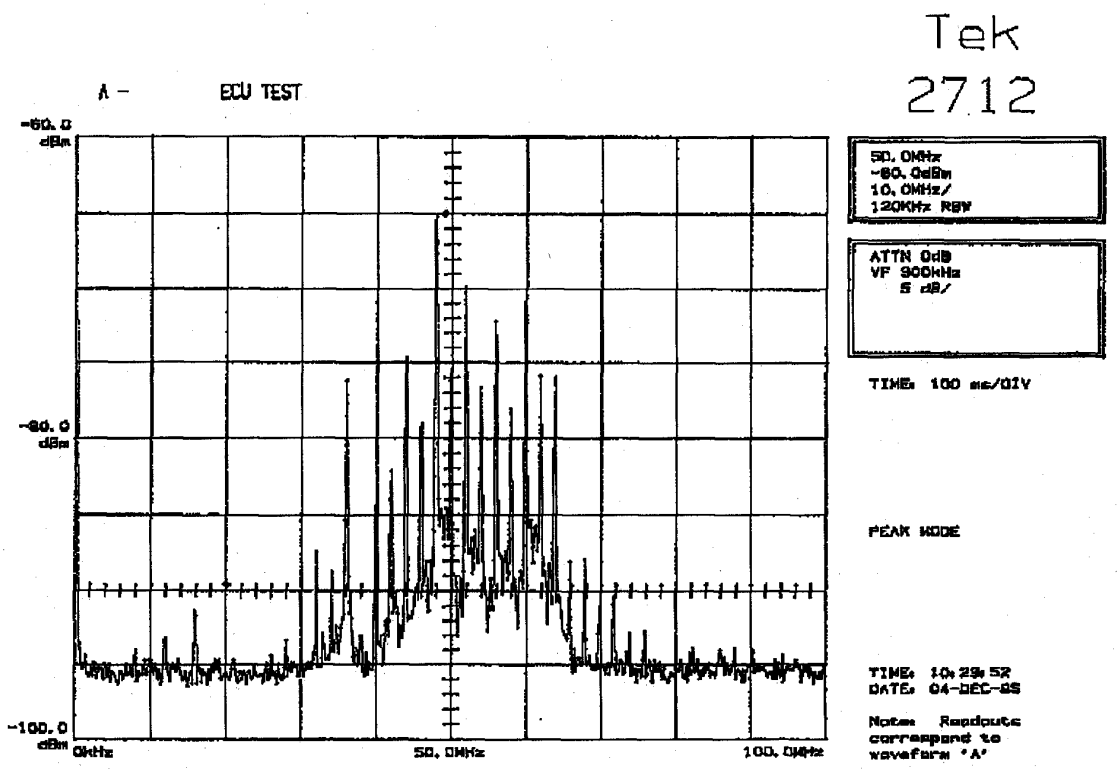

Fig. 11. Common-mode current measured on the power and photocell input cable bundle.

paths in proximity. Measurements were taken at several points between the power pins of the single on-board IC module and the photocell input pin at the connector. Significant noise over the entire 100 MHz band was measured, with a slight peaking around 50 MHz. A 0.1 μF decoupling capacitor was placed at the connector across the photocell input and ground, as indicated in Fig. 10(b). The addition of the decoupling capacitor between the photocell input and ground decreased the measured common-mode current by at least 30 dB. The dynamic range of the measurements is only 30 dB (initial common-mode current above the noise floor), and it is possible that the common-mode current decreased even further. Both surface-mount and leaded 0.1 μF capacitors were employed and found to produce the same results within the dynamic range of the measurements.

The dominant EMI source mechanism was voltage-driven. A simple model of the equivalent noise source and antenna on the DRL module is shown in Fig. 10(b). The driving source for the antenna was the differential-mode noise voltage on the 5 V power bus. The noise voltage was developed between the photocell input lead and ground as a result of the IC module switching (delta-I noise). The differential-mode source ultimately resulted in common-mode current on the photocell input and power lead cable bundle. The antenna was comprised of the photocell input lead and the extensive metal structures of several on-board relays that were directly connected to ground, as well as imbalances in the attached cable and the extended power ground.

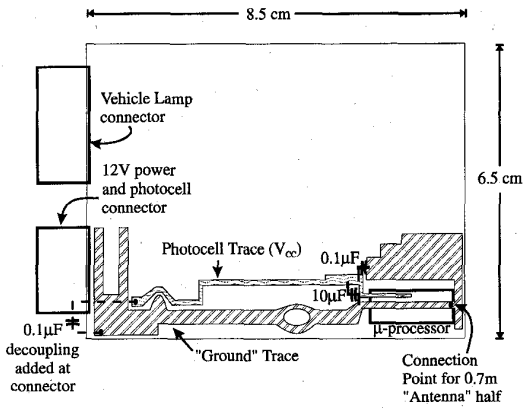

Fig. 12. Partial layout diagram of the DRL module showing the location of the photocell trace, ground trace, decoupling capacitors, connectors, and microprocessor.

The measured common-mode current on the described cable bundle for the off-the-shelf configuration of the DRL module was found to be predominantly due to a voltage-driven mechanism. Further inspection of the reduced circuit model of Fig. 10(b) indicates that the decoupling capacitor loop can provide a current-driven EMI source mechanism denoted by V_{CM}. The large switching currents drawn by the IC module will produce a voltage drop along the ground conductor that can potentially drive two portions of the ground against one another (as two conductors of an antenna). The

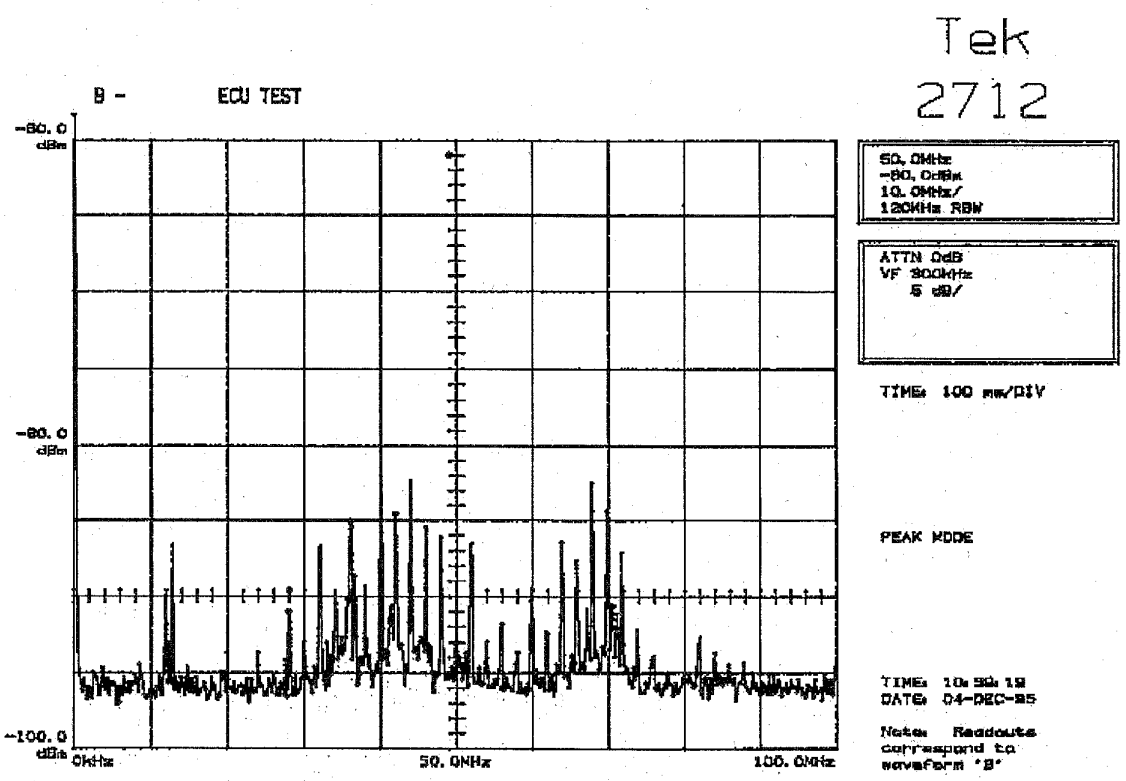

Fig. 13. Common-mode current measured on the photocell input and power lead cable bundle with a 0.7 m wire attached to the ground conductor on the side of the IC package opposite the connector, and 100 nF decoupling between the photocell input and ground at the connector.

equivalent noise-voltage source V_{CM} that results from the differential-mode switching current is further increased in the attempt to eliminate the voltage-driven mechanism by placing a decoupling capacitor between the photocell input lead (connected to V_{CC}) and ground at the connector. The length of the differential-mode loop is increased, as is possibly the differential mode-current by the addition of the 0.1 μF capacitor across the photocell input and ground leads of the connector. The current path is increased and the voltage dropped along the return conductor increases. The RF noise at four points along the ground conductor was measured with a 0.085 in semi-rigid coaxial-cable probe with a 0.1 μF decoupling capacitor connected between the photocell input lead and ground at the connector. A considerable difference in the magnitude of the RF noise over the extent of the differential-mode switching-current loop was measured. This variation in the noise on the ground is consistent with a current-driven mechanism.

Fig. 12 shows a partial diagram of the PCB layout. The vehicle lamp connector was used to route high current from solenoids on the board to the various lighting systems on the vehicle and had no I/O signals from the microprocessor. The decoupling capacitor loop, and the loop with the added 0.1 μF (between the photocell lead and ground at the connector as shown in Fig. 12) provides an EMI source mechanism that can drive an antenna. However, the judicious placement of the IC module in the far corner of the printed circuit board effectively placed the equivalent noise voltage source very close to the end of the potential antenna. The high input impedance associated with an end-driven source results in unmeasurable common-mode current. A lower input impedance antenna can be artificially provided by connecting a wire to the ground conductor on the side of the IC package opposite the connector as shown in Fig. 12. This places the equivalent noise-voltage source produced by the differential-mode current approximately in the middle of the antenna, thereby lowering the input impedance. The common-mode current measured on the photocell input and power lead bundle for this configuration is shown in Fig. 13. Significant common-mode current on the cable bundle results around 40 and 60 MHz.

VI. Discussion

Two EMI source mechanisms by which common-mode current can be induced on cables attached to PCB's have been investigated. These mechanisms are related to differential-mode voltages and currents on the PCB or at the connector. It was shown numerically and experimentally that depending on the "antenna" which is being driven and the signal levels, either mechanism can dominate. Because of the different nature of the current- and voltage-driven mechanisms, the approach to minimizing common-mode radiation problems depends on the dominant mechanism. Changes in the circuit that decreases CM radiation due to one mechanism could, in some cases, increase the CM current as a result of the other mechanism.

The numerical, passive circuit, and active production circuit examples given in the previous sections were simple in order to demonstrate the fundamental physics and aspects of

EMI. However, many EMI problems for state-of-the-art high-speed digital designs can be significantly more complicated. A knowledge of fundamental source mechanisms, though, provides a powerful tool for identifying PCB layout geometries that are potential EMI sources, coupling paths, and antennas. Common layout configurations that are potential EMI sources and coupling paths can be identified, and appropriate equivalent circuit and antenna models can be constructed in order to develop guidelines to avoid EMI problems at the design stage. Further, the source mechanisms, coupling paths, and antennas identified in designs can be analyzed using analytical numerical modeling techniques to investigate potential EMI problems without the need for modeling extraneous board features.

ACKNOWLEDGMENT

The authors would like to thank Lindgren RF Enclosures for the donation of a shielding enclosure and Fischer Custom Communications for donating current probes that greatly facilitated this research.

REFERENCES

[1] C. R. Paul and D. R. Bush, "Radiated emissions from common-mode currents," in *Proc. 1987 IEEE Int. Symp. Electromag. Compat.*, Atlanta, GA, Sept. 1987, IEEE Electromag. Compat. Soc., pp. 197–203.

[2] C. R. Paul, "A comparison of the contributions of common-mode and differential-mode currents in radiated emissions," *IEEE Trans. Electromag. Compat.*, vol. 31, pp. 189–193, May 1989.

[3] T. Hubing and J. F. Kaufman, "Modeling the electromagnetic radiation from electrically small table-top products," *IEEE Trans. Electromag. Compat.*, vol. 31, pp. 74–84, Feb. 1989.

[4] K. B. Hardin and C. R. Paul, "Decompisition of radiating structures using the ideal structure extraction method (ISEM)," *IEEE Trans. Electromag. Compat.*, vol. 35, pp. 274–273, May 1993.

[5] M. Radojicic and G. Costache, "A model to predict radiated emissions from electronic circuits," in *Proc. IEEE Int. Symp. Electromag. Compat.*, Cherry Hill, NJ, 1991, IEEE Electromag. Compat. Soc., pp. 50–57.

[6] R. W. Dockey, "Asymmetrical mode radiation from multilayer printed circuit boards," in *EMC/ESD Int. Symp. Dig.*, Apr. 1992, pp. 247–251.

[7] R. W. Dockey and R. F. German, "New techniques for reducing printed circuit board common-mode radiation," in *Proc. 1993 IEEE Int. Symp. Electromag. Compat.*, Dallas, TX, Aug. 1993, IEEE Electromag. Compat. Soc., pp. 334–339

[8] J. L. Drewniak, T. H. Hubing, and T. P. Van Doren, "Investigation of fundamental mechanisms leading to common-mode radiation from printed circuit boards with attached cables," EMC Lab, University of Missouri-Rolla, Tech. Rep. TR93-4-012R, May 1993.

[9] ——, "Investigation of fundamental mechanisms of common-mode radiation from printed circuit boards with attached cables," in *Proc. 1994 IEEE Int. Symp. Electromag. Compat.*, Chicago, IL, Aug. 1994, IEEE Electromag. Compat. Soc., pp. 110–115.

[10] J. R. Bergervoet, "EMC measurements and models connecting the system level with the module level," *Phillips J. Res.*, vol. 48, pp. 63–80, 1994.

[11] J. L. Drewniak, F. Sha, T. H. Hubing, T. P. Van Doren, and J. Shaw, "Diagnosing and modeling common-mode radiation from printed circuit boards with attached cables," in *Proc. 1995 IEEE Int. Symp. Electromag. Compat.*, Chicago, IL, Aug. 1995, IEEE Electromag. Compat. Soc., pp. 465–470.

[12] D. M. Hockanson, C.-W. Lam, J. L. Drewniak, T. H. Hubing, and T. P. Van Doren, "Experimental and numerical investigations of fundamental radiation mechanisms in PCB designs with attached cables," in *Proc. IEEE Int. Symp. Electromag. Compat.*, Santa Clara, CA, 1996, IEEE Electromag. Compat. Soc., pp. 305–310.

[13] G. J. Burke and A. J. Poggio, *Numerical Electromagnetics Code (NEC)—Method of Moments: User's Manual*, Jan. 1981.

[14] C. R. Paul, *Introduction to Electromagnetic Compatibility*. New York: Wiley, 1992.

David M. Hockanson (S'96) received the B.S. and M.S. degrees in electrical engineering from the University of Missouri, Rolla, in 1992 and 1994, respectively. His undergraduate and graduate education has been supported by scholarships and fellowships, and he is currently supported by a National Science Foundation Graduate Fellowship.

His research interests include numerical and experimental analysis of electromagnetic compatibility problems. Previous work has involved digital power bus design and shielding enclosure design. Presently, he is working on experimental investigations and equivalent circuit development of noise sources and radiation mechanisms on printed circuit board geometries.

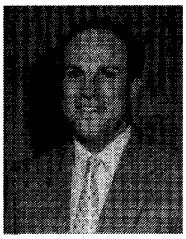

James L. Drewniak (S'85–M'90) received the B.S. (highest honors), M.S., and Ph.D. degrees in electrical engineering from the University of Illinois, Urbana-Champaign, in 1985, 1987, and 1991, respectively. He pursued graduate studies in wave propagation and interactions in the areas of electromagnetics, antennas, microwaves, and acoustics.

In July 1991, he joined the Electrical Engineering Department at the University of Missouri, Rolla, as an Assistant Professor. His research interests include the development and application of numerical methods for investigating electromagnetic compatibility problems, antenna analysis, and modeling of microwave components, as well as experimental studies in antenna and electromagnetic compatibility problems.

Dr. Drewniak is the Secretary/Treasurer of the Rolla IEEE Subsection and an Associate Editor for the *Applied Compuational Electromagnetics Society Newsletter*.

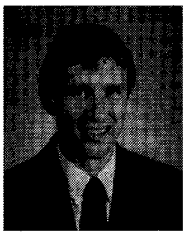

Todd H. Hubing (S'82–M'83–SM'93) received the B.S.E.E. degree from the Massachusetts Institute of Technology in 1980, an M.S.E.E. degree from Purdue University in 1982, and a Ph.D. degree in electrical engineering from North Carolina State University in 1988.

From 1982 to 1989, he was employed in the Electromagnetic Compatibility Laboratory at IBM Communications Products Division in Research Triangle Park, NC. He is currently an Associate Professor of electrical engineering at the University of Missouri, Rolla. Since joining the university in 1989, he has earned an Outstanding Teaching Award and two awards for faculty excellence. His primary area of research involves the development and application of numerical methods for solving problems in electromagnetic compatibility.

Dr. Hubing is the Director of Member Services for the IEEE EMC Society and the Treasurer of the Applied Computational Electromagnetics Society. He also writes the "Chapter Chatter" column for the IEEE EMC Society Newsletter.

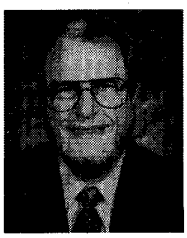

Thomas P. Van Doren (S'60–M'69) received the B.S., M.S., and Ph.D. degrees from the University of Missouri, Rolla, MO, in 1962, 1963, and 1969, respectively.

From 1963 to 1965, he served as an Officer in the U.S. Army Security Agency. From 1965 to 1967, he was a Microwave Engineer with Collins Radio Company. Since 1967, he has been a member of the electrical engineering faculty at the University of Missouri, Rolla, where he is currently a Professor. His research interests concern developing circuit layout, grounding, and shielding techniques to improve electromagnetic compatibility. He has taught short courses on electromagnetic compatibility to more than 10 000 engineers and technicians representing 200 corporations.

Dr. Van Doren received an IEEE EMC Society Richard R. Stoddard Award for his contributions to EMC research and education in 1995. He is a registered Professional Engineer in the state of Missouri and a member of Eta Kappa Nu, Tau Beta Pi, and Phi Kappa Phi.

Fei Sha (M'91) was born in Shanghai, China. He received the degree in physics from Fudan University, Shanghai, China, in 1967 and the M.S.E.E. degree from Northern Jiaotong University, Beijing, China, in 1983.

He is currently an Associate Professor in the Department of Communication and Control Engineering at the Northern Jiaotong University. He was a Visiting Scholar in the Department of Electric Engineering at the University of Missouri, Rolla, from 1993 to 1996. He has been working in the field of EMC since 1983. His research interests include intersystem and intrasystem noise prediction and control, and EMC test methods.

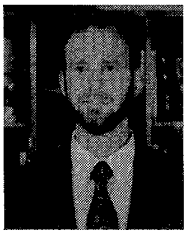

Michael J. Wilhelm received the B.S.E.E. and M.S.E.E. degrees from the University of Missouri, Rolla, in 1992 and 1994, respectively. Prior to receiving the degrees, he served four years as a radio repairman in the U.S. Marine Corps, two years in industrial electronics service, and three years as a technician for Sherwood Medical Inc.

Currently, he is an RF design engineer for Motorola's Cellular Infrastructure Group where his principal responsibility is the design of LNA's for cellular base stations.